RAA 2016 Vol. **16** No. **1**, 20 (15pp) doi: 10.1088/1674–4527/16/1/020
http://www.raa-journal.org *http://iopscience.iop.org/raa*

Research in Astronomy and Astrophysics

Non-ballistic motion and precessing helical trajectory in quasar NRAO 150

Shan-Jie Qian

National Astronomical Observatories, Chinese Academy of Sciences, Beijing 100012, China; *rqsj@bao.ac.cn*

Received 2015 January 1; accepted 2015 July 15

Abstract NRAO 150 is a very special radio quasar in which prominent non-ballistic superluminal motion has been observed in its inner-jet region. We apply model-fittings to the kinematics of the superluminal knots (trajectory, distance from the core and apparent velocity) in terms of a helical precessing jet-nozzle model. Five cases are considered in which the angle between the jet axis and the line of sight is assumed to be 6°, 3°, 1°, 0.6° and 0.12°, respectively. It is shown that the superluminal components have intrinsic acceleration in the innermost regions ($\lesssim 0.2$ mas from the core). The phenomenon of precessing nozzle/trajectory can be understood on the basis of relativistic magnetohydrodynamic theories for relativistic jets.

Key words: radio continuum: galaxies — galaxies: jets — galaxies: kinematics — galaxies: individual (quasar NRAO 150)

1 INTRODUCTION

NRAO 150 is a very bright radio to mm quasar at a high redshift ($z = 1.517$), which was measured through near-IR spectroscopic observation (detection of the Hα and Hβ spectral lines) by Acosta-Pulido et al. (2010). On scales observable by very long baseline interferometry (VLBI), it displays a compact core-jet structure. Recently it has been monitored at 86 and 43 GHz with sub-milliarcsecond resolution by Agudo et al. (2007) during the period of 1997–2007. They found this source to have remarkable properties: (1) large misalignment of $> 100^\circ$ between the mm-jet and the cm-jet (Fey & Charlot 2000); (2) in the inner region (less than $\sim$0.5 mas) three superluminal components (Q_1, Q_2 and Q_3) moving non-ballistically and having very curved trajectories; (3) the three superluminal components having extremely fast counterclockwise rotation of their position angle with a rate of $\sim 6^\circ$–11° yr^{-1}; (4) their apparent superluminal speeds are: total velocity between 2.3c and 3.3c, and non-radial velocity between 2.7c and 1.4c. Thus NRAO 150 is an extreme case that exhibits jet position angle swing and non-ballistic motion which are worth studying in detail. Recently, Molina et al. (2013, 2014) carried out detailed multi-frequency VLBI polarimetric observations between 2006–2010 and found the toroidal field structure in the innermost regions of the source. Combining the new and previous evidence, they proposed an internal jet rotation model to explain the kinematics of the superluminal knots with the jet being seen face-on.

Jet position angle swings have been detected in a number of blazars (e.g. 3C345, 3C279, 3C454.3, 3C273, OJ287 and BL Lacertae) and their physical origin is not fully understood. A few mechanisms have been proposed to explain this phenomenon: (1) jet precession caused by disk-precession or orbital motion in a binary black hole system (e.g. Tateyama & Kingham 2004, Lobanov & Roland 2005); (2) precession of the jet nozzle from which superluminal components are ejected (e.g. Tateyama & Kingham 2004, Stirling et al. 2003, Lister et al. 2003, Qian et al. 2014, Qian 2013, 2012, 2011; Qian et al. 2009, Qian et al. 1992, Steffen et al. 1995, Villata et al. 1998, Villata & Raiteri 1999); (3) jet-disk instabilities causing erratic swings (e.g. Agudo 2009, Agudo et al. 2012, Lu et al. 2013).

In this paper, we will study the jet position angle swing (wobbling) in the quasar NRAO 150 by applying the precessing helical jet-nozzle model (suggested for blazar 3C345 by Qian et al. 1992) to fit its VLBI-kinematics (trajectory, core-distance and apparent velocity of its three superluminal knots observed at a wavelength of 7 mm by Agudo et al. 2007) and their kinematic parameters (bulk Lorentz/Doppler factor and viewing angle) are derived. The precessing (helical or collimated) jet-nozzle model has also been applied to fit the model for the ejection position angle swings observed in blazars 3C279 and 3C454.3 (Qian et al. 2009; Qian 2011, 2012, 2013; Qian et al. 2014). When taking into account the rotation of the inner trajectory of the knots around the jet-axis, this approach is helpful for studying the precession of the inner jet structure and the extended intrinsic acceleration that occurred within the inner jet regions. The source NRAO 150 is another example of a precessing helical jet-nozzle, as discussed below.

In this paper we will adopt the concordant cosmological model with Ω_λ = 0.7, Ω_m = 0.3 and Hubble constant H_0 = 70 km s^{-1} Mpc^{-1} (Spergel et al. 2003). Thus for NRAO 150, $z = 1.517$, its luminosity distance is $D_{\rm L}$ = 11.07 Gpc (Hogg 1999; Pen 1999) and angular distance $D_{\rm A}$ = 1.748 Gpc. Angular scale 1 mas = 8.484 pc and proper motion of 1 mas yr^{-1} are equivalent to an apparent

velocity of $69.5c$. In the galaxy frame, $1c$ is equivalent to 0.03622 mas yr^{-1}.

The plan of this paper is: Section 2 describes the formalism of the model; Section 3 gives the description of helical trajectory; Section 4 gives the model-fitting applied to kinematics; Section 5 describes the discussion and conclusions.

2 FORMALISM OF THE MODEL

In order to develop our precession model for the superluminal ejection of the knots in NRAO 150, we first describe the formalism (following Qian et al. 1992, 2009).

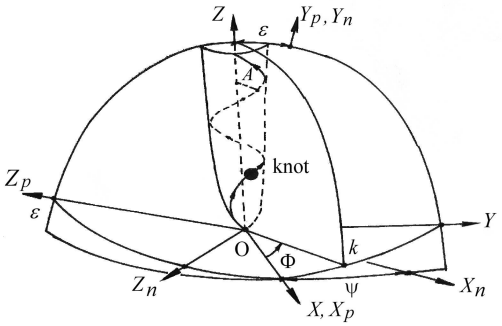

Fig. 1 Geometry of the model for fitting the kinematics of the superluminal components in the quasar NRAO 150.

The geometry of the model is shown in Figure 1, in which three coordinate systems are shown: (X, Y, Z), (X_p, Y_p, Z_p) and (X_n, Y_n, Z_n). Axis Y_n is directed toward the observer and (X_n, Z_n) defines the plane of the sky with the axis X_n directed toward the negative right ascension and axis Z_n the north pole (declination). Axis Z represents the jet-axis defined by parameters (ϵ, ψ). The trajectory of a superluminal knot is described by cylindrical coordinates ($A(Z)$, $\Phi(Z)$, Z), where Z is the distance from the origin along the jet-axis. $A(Z)$ represents the amplitude of the knot's path and $\Phi(Z)$ is the azimuthal angle or the phase of the knot. When functions $A(Z)$, $\Phi(Z)$, ϵ and ψ and bulk Lorentz factor Γ are given, the kinematics of the knot (trajectory, apparent velocity, Doppler factor and viewing angle as functions of time) can be calculated. The relevant formulas are listed as follows.

$$X(Z,\Phi) = A(Z)\cos\Phi\,, \tag{1}$$

$$Y(Z,\Phi) = A(Z)\sin\Phi\,. \tag{2}$$

The projection of the trajectory on the sky plane is represented by

$$X_n(Z,\Phi) = X_p(Z,\Phi)\cos\psi - Z_p(Z,\Phi)\sin\psi\,, \tag{3}$$

$$Z_n(Z,\Phi) = X_p(Z,\Phi)\sin\psi + Z_p(Z,\Phi)\cos\psi\,, \tag{4}$$

where

$$X_p(Z,\Phi) = X(Z,\Phi)\,, \tag{5}$$

$$Z_p(Z,\Phi) = Z\sin\epsilon - Y(Z,\Phi)\cos\epsilon\,. \tag{6}$$

We give the formula for viewing angle θ, Doppler factor δ, apparent transverse velocity β_a and elapsed time T_0 after ejection:

(1) Viewing angle

$$\theta = \arccos[\cos\epsilon(\cos\Delta + \sin\epsilon\tan\Delta_p)]\,, \tag{7}$$

where

$$\Delta = \arctan\left[\left(\frac{dX}{dZ}\right)^2 + \left(\frac{dY}{dZ}\right)^2\right]^{1/2}, \tag{8}$$

Δ is the angle between the spatial velocity vector and Z-axis, and

$$\Delta_p = \arctan\left(\frac{dY}{dZ}\right), \tag{9}$$

is the projection of Δ on the (Y,Z)-plane.

(2) Apparent transverse velocity and Doppler factor

$$v_a = c\beta_a = \frac{c\beta\sin\theta}{1-\beta\cos\theta}\,, \tag{10}$$

$$\delta = \frac{1}{\Gamma(1-\beta\cos\theta)}\,, \tag{11}$$

where $\beta = \frac{v}{c}$, v is the spatial velocity of the knot and $\Gamma = (1-\beta^2)^{-1/2}$ is the Lorentz factor.

(3) Elapsed time

$$T_0 = \int_0^Z \frac{1+z}{\Gamma\delta v\cos\Delta_s}dZ\,, \tag{12}$$

where

$$\Delta_s = \arccos\left[\left(\frac{dX}{dZ}\right)^2 + \left(\frac{dY}{dZ}\right)^2 + 1\right]^{-1/2}. \tag{13}$$

Here z is the redshift of NRAO 150.

All coordinates and amplitude are measured in units of mas (milliarcsecond) and Φ is measured in units of radian (rad).

3 DESCRIPTION OF HELICAL TRAJECTORY

In the case of NRAO 150, we adopt the pattern of helical trajectory similar to that chosen for fitting the kinematics of superluminal motion in quasar 3C345 (Qian et al. 2009). The amplitude $A(Z)$ and phase $\Phi(Z)$ of the helical trajectory as a function of Z is taken as follows. We choose simple functions to describe the helical paths of the superluminal knots. Since the VLBI observations given by Agudo et al. (2007) only show the kinematics beyond core distance $>$0.1 mas, our model can only be used to fit the kinematics of NRAO 150 after 1997.0. The functions $A(Z)$ and $\Phi(Z)$ are chosen as follows.

For $Z \le 0.03$ mas

$$\begin{aligned} A(Z) &= aZ\,, \\ \Phi(Z) &= \Phi_0 - \phi + \eta R_\phi Z\,, \end{aligned} \tag{14}$$

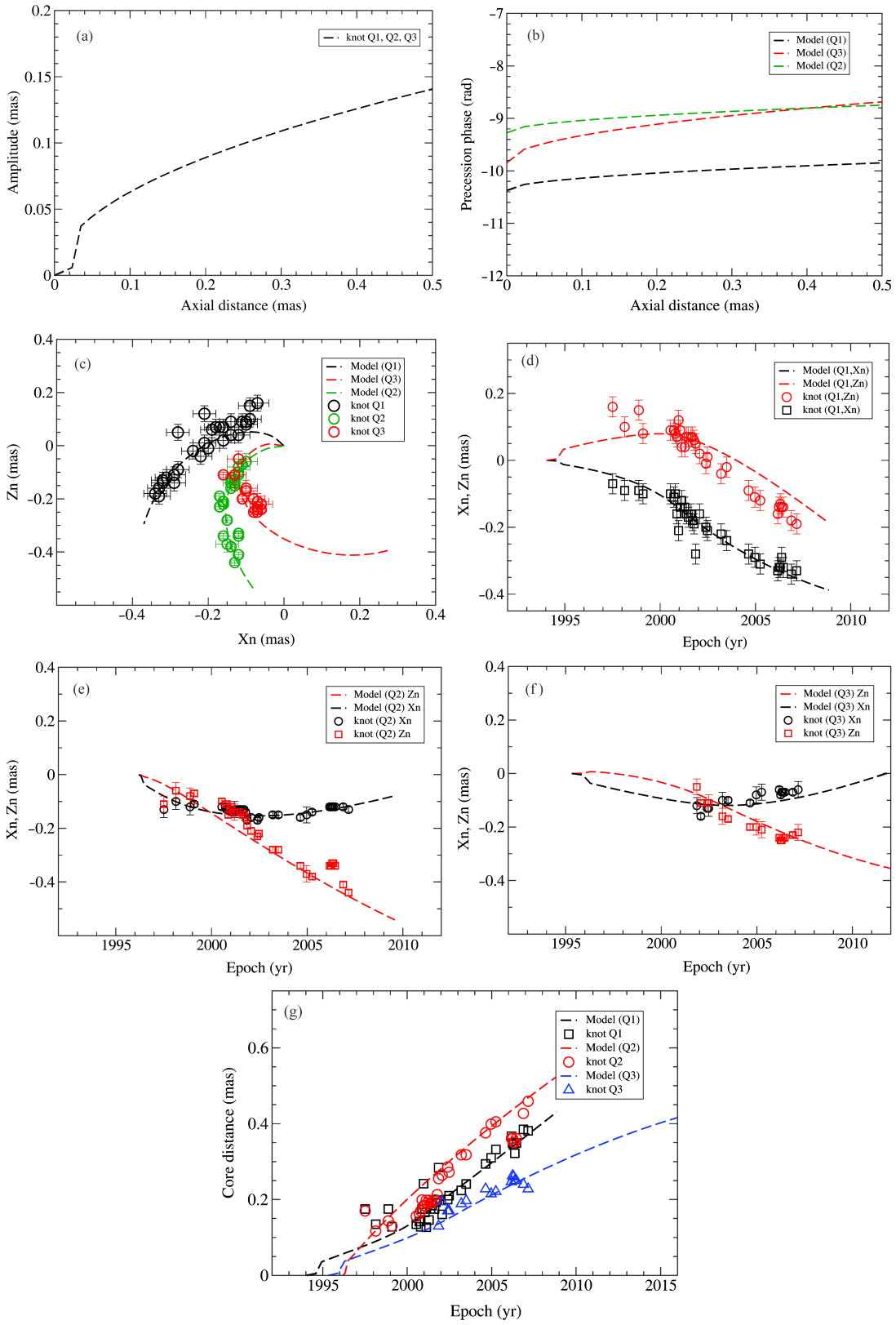

Fig. 2 Fitting results for $\epsilon = 3°$: Amplitude $A(Z)$ and phase $\Phi(Z)$; trajectory (X_n, Z_n), $X_n(t)$ and $Z_n(t)$ (respectively for Q1, Q2 and Q3); and core distance.

ϕ is defined as the phase of ejection of the knot. Parameter R_ϕ introduced in the model describes the rotation of the trajectory. Φ_0 and a are constants.

For $Z > 0.03$ mas

$$A(Z) = b(\sin(\pi Z/Z_1))^{1/2}, \quad \Phi(Z) = \Phi_0 - \phi + \eta(Z/Z_2)^{1/2}. \tag{15}$$

We will take $a = 0.2512$, $b = 0.55$ mas, Φ_0 = 5.891 rad and R_ϕ = 4.992 rad mas^{-1}. Parameters Z_1 and Z_2 will be chosen for different cases (corresponding to different ϵ), and η and ϕ will be chosen for different knots.

4 MODEL FITTING APPLIED TO KINEMATICS.

In this paper we will consider the possibility of whether the kinematics of superluminal knots ejected from NRAO 150 can be fitted by the precessing jet-nozzle model proposed for explaining the jet position angle swings in blazars like 3C345, 3C454.3 and 3C279 (Qian et al. 2014, Qian 2013, 2012, 2011; Qian et al. 2009, Qian et al. 1992). We will apply 3-dimensional simulations of a helical trajectory for fitting the curved trajectories observed in NRAO 150. We emphasize that an effective model should reasonably and consistently fit the trajectory, core distance (or core separation) and apparent superluminal speed. We have applied model simulations for five cases that have different values of ϵ (the angle between the jet-axis and the line of sight): $\epsilon = 6^\circ$, 3°, 1°, 0.6° and 0.12° (ψ = 1.6958 rad (arbitrary)) in order to show the effects from different viewing angles and various radial distance scales. The VLBI data (1997–2007, 43 GHz) for the superluminal knots observed in NRAO 150 are taken from Agudo et al. (2007). This dataset (acquired during 1997–2007) contains four components (Q0, Q1, Q2 and Q3) and knot Q0 was assumed to be the stationary core while components Q1, Q2 and Q3 exhibited superluminal motions. In the jet rotation model, Molina et al. (2013, 2014) chose a new reference point as the core position by assuming component Q0 is also superluminal. Since the dataset (only during 2006–2010) given by Molina et al. did not contain the data for the four components (during 1997–2007) after the change of the core position, we can only use the dataset given by Agudo et al. (2007) for our model simulations for knots Q1, Q2 and Q3. However, this would not limit the implications of the simulations given here. We should point out that our method of model simulation defined in terms of the helical precessing jet nozzle scenario (e.g. Qian et al. 1992, Qian et al. 2014) is quite flexible and it would be not difficult to simulate the curved trajectories of the four components (Molina et al. 2014) if related data are available.

In the following we will show the results of our model-fitting. For clearly demonstrating the essential information, the fitting results of trajectory, core distance and apparent velocity are only shown for two cases ($\epsilon = 3^\circ$ and 0.12°) as an illustration. The fitting results for the other three cases ($\epsilon = 6^\circ$, 1° and 0.6°) are provided in the Appendixes. Thus a concrete comparison between the results for different viewing angles (e.g. intrinsic extended acceleration and required Lorentz/Doppler factor at different radial distances) could be made if necessary.

4.1 Results for $\epsilon = 3^\circ$

The parameters used for the model-fitting are:
Z_1 = 24 mas and Z_2 = 1.8 mas. The amplitude and precession phase functions are described by Equations (14) and (15) as shown above. The respective model parameters for knots Q1, Q2 and Q3 are given as follows.

- Knot Q1: Ejection epoch t_0 = 1994.04, ϕ = 4.0 rad and η = 1. Initial intrinsic acceleration is required in order to consistently fit the trajectory, core-distance and apparent velocity: for $Z \leq 0.8$ mas, $\Gamma = 1.5 + (4.0 - 1.5)Z/0.8$ and for $Z > 0.8$ mas, Γ = 4.0.
- Knot Q2: Ejection epoch t_0 = 1996.20, ϕ = 2.6 rad and $\eta = 1$. No intrinsic acceleration is assumed: Γ = 3.7.
- Knot Q3: Ejection epoch t_0 = 1995.319, ϕ = 3.17 rad and η = 2.2 (more rotation than for knots Q1 and Q2). Intrinsic acceleration is taken as: for $Z \leq 0.5$ mas $\Gamma = 1.5 + (2.7 - 1.5)Z/0.5$ and for $Z > 0.5$ mas Γ = 2.7.

The fitting results are shown in Figures 2–3. Some properties can be inferred: For knots Q1 and Q3 intrinsic acceleration is required in order to fit their kinematics. The trajectory, core-distance and apparent velocity are reasonably and consistently well fitted for the three knots. The fitted Lorentz factors are in the range of ∼2–4. The modeled viewing angles are in the range of 8°–20°. In this case the precession period is derived to be 9.70 yr.

4.2 Results for $\epsilon = 0.12^\circ$

The parameters used for the model fitting are:
Z_1 = 330 mas and Z_2 = 18 mas. The amplitude and phase functions are described by Equations (14) and (15) as shown above. The respective parameters for knots Q1, Q2 and Q3 are given as follows.

- Knot Q1: Ejection epoch t_0 = 1996.0, ϕ = 4.0 rad, η = 1. The intrinsic acceleration is chosen as: for $Z \leq 4.0$ mas, $\Gamma = 3.5 + (12.6 - 3.5)Z/4.0$ and $Z > 4.0$ mas, Γ = 12.6.
- Knot Q2: Ejection epoch t_0 = 1996.30, ϕ = 2.8 rad, η = 1. The intrinsic acceleration is chosen as: for $Z \leq 3.0$ mas, $\Gamma = 3.8 + (12.3 - 3.8)Z/3.0$; for $Z > 3.0$ mas, Γ = 12.3.
- Knot Q3: Ejection epoch t_0 = 1996.15, ϕ = 3.40 rad, η = 2.3 (larger rotation rate than for Q1 and Q2). Intrinsic acceleration is assumed as: for $Z \leq 2.0$ mas, $\Gamma = 3.1 + (8.5 - 3.1)Z/2.0$ and for $Z > 2.0$ mas, Γ = 8.5.

The model-fitting results are shown in Figures 4 and 5. It can be seen that the trajectory, distance from the core and apparent velocity can be reasonably and consistently

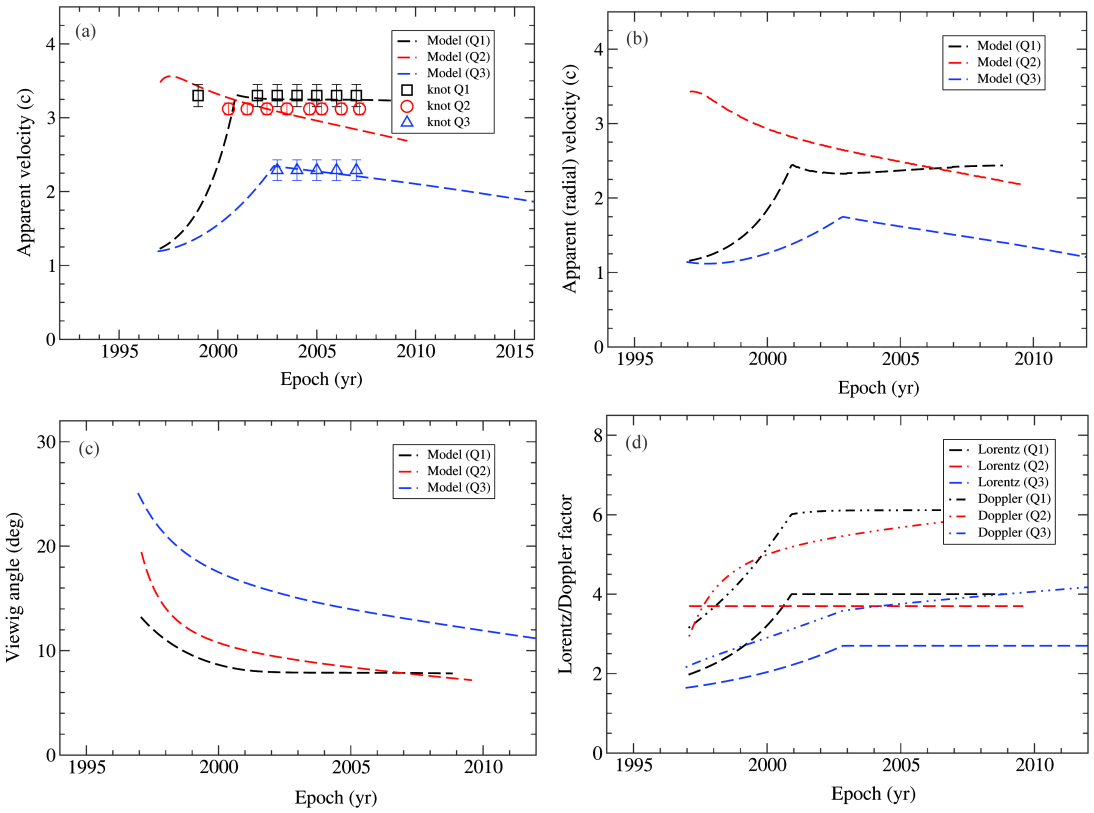

Fig. 3 Model-fitting results for $\epsilon = 3°$: apparent total and radial velocity, modeled viewing angle and Lorentz/Doppler factor. There are different values for the modeled viewing angle and bulk Lorentz/Doppler factor.

well fitted for the three knots by the model. The modeled Lorentz factors are in the range of ∼4–13 and the Doppler factors in the range of ∼8–25. The modeled viewing angles are in the range of $\sim 0.5°$–$3°$. The precession period is derived to be 1.57 yr (in the galaxy frame this is 0.6 yr). This case ($\epsilon = 0.12°$) might be regarded as an approximation to the face-on viewing discussed by Molina et al. (2014). We find that for all the three components (Q1, Q2 and Q3) initial intrinsic accelerations within radial distances ∼2-4 mas (or 17–34 pc from the galaxy center) are required such that bulk Lorentz factor (Γ) ranges from ∼4 to ∼12; see Table 1.

5 DISCUSSION AND CONCLUSION

We have used the precessing helical jet nozzle model proposed by Qian et al. (1992, 2009, 2014) to apply model-fittings to the kinematics of the superluminal knots Q1, Q2 and Q3 observed in quasar NRAO 150. Their trajectory (including (X_n, Z_n), $X_n(t)$, $Z_n(t)$), core-distance and apparent velocity (including total and radial velocity) are all reasonably and consistently well fitted. Their bulk Lorentz factor, Doppler factor and viewing angle are derived (figs. 2 to 11). Intrinsic accelerations are required in the innermost regions (core separations (or core distances) $\lesssim$0.2 mas).

The results for the five cases of the angle between the jet-axis and the line of sight ($\epsilon = 6°$ to $0.12°$) consistently demonstrate that the extremely non-ballistic motion of the superluminal components (Q_1, Q_2 and Q_3) and the rapid rotation of their direction of ejection (or jet position angle swing on the the plane of the sky) can be interpreted in terms of this scenario. In the model fitting we intended to arrange the three components (Q_1, Q_2 and Q_3) ejected in order of time with their phases satisfying the corresponding period of precession, although three components are just enough to derive a period. Thus our model-fitting results show that the superluminal knots observed in NRAO 150 could move along a common helical path which precesses around the jet-axis and could exhibit a regular (or quasi-periodic) behavior during the observing period (∼1997–2007). This might imply an enduring stable structure of a magnetic field very close to the central black-hole/accretion disk where the jet is formed, accelerated and collimated.

Additionally, we find that the model-fitting simulations require intrinsic acceleration of the knots. Table 1 gives the fitting results of intrinsic acceleration of the knots (Q1, Q2 and Q3) for the cases of $\epsilon = 6°$, $3°$, $1°$, $0.6°$ and $0.12°$, showing the radial distance of the acceleration regions and the range of resulting Lorentz factors. It can be seen that for the cases $\epsilon = 0.6°$ and $\epsilon = 0.12°$ significant intrinsic acceleration is required (Lorentz factor Γ ranges from 3 to 6 and from 3 to 10 respectively) and the acceleration region could extend to ∼20–30 pc. Extended intrinsic acceleration of superluminal knots has

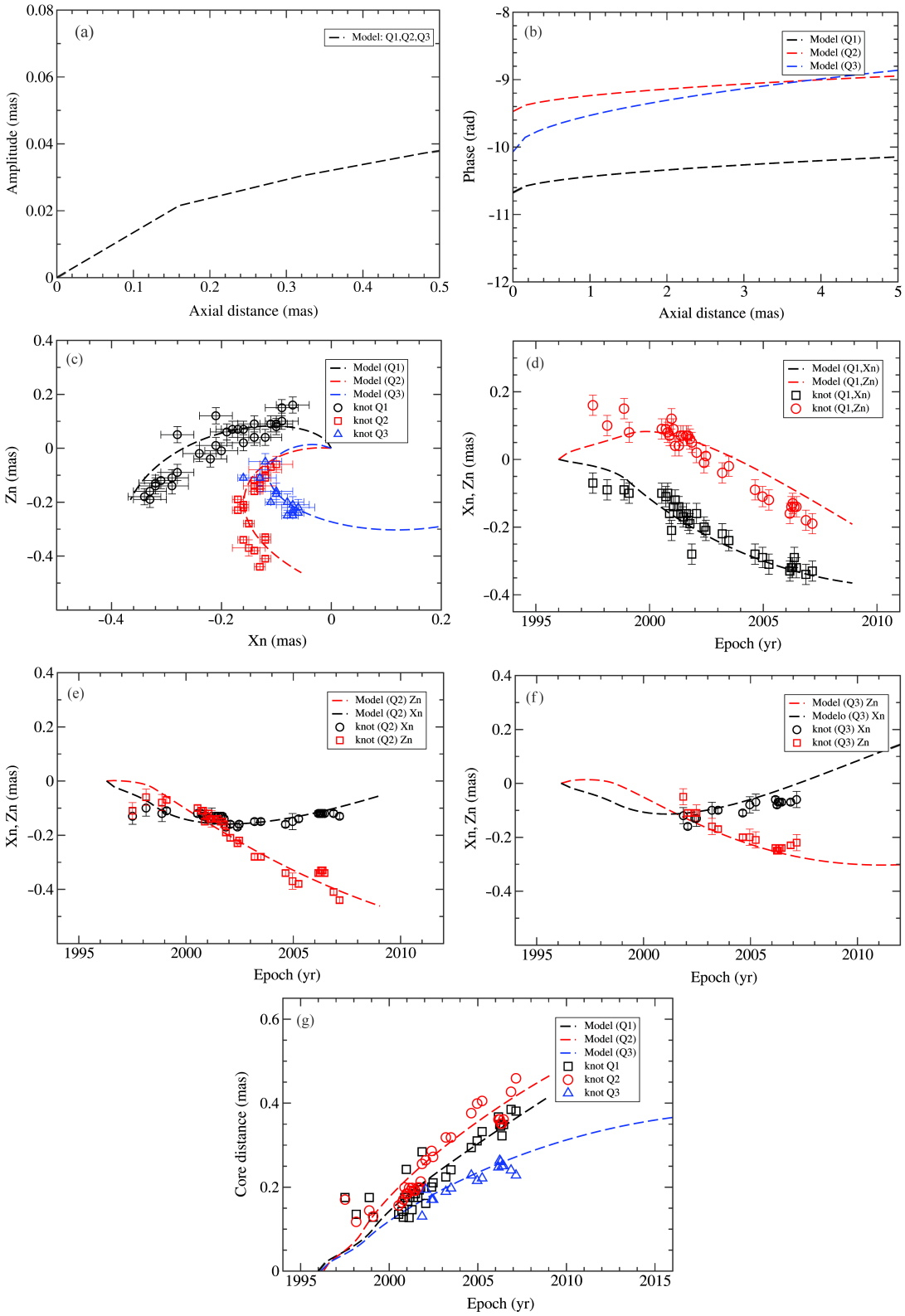

Fig. 4 Fitting results for $\epsilon = 0.12°$. Amplitude $A(Z)$ and phase $\Phi(Z)$, trajectory (X_n, Z_n), $X_n(t)$ and $Z_n(t)$ (respectively for Q1, Q2, Q3) and core distance.

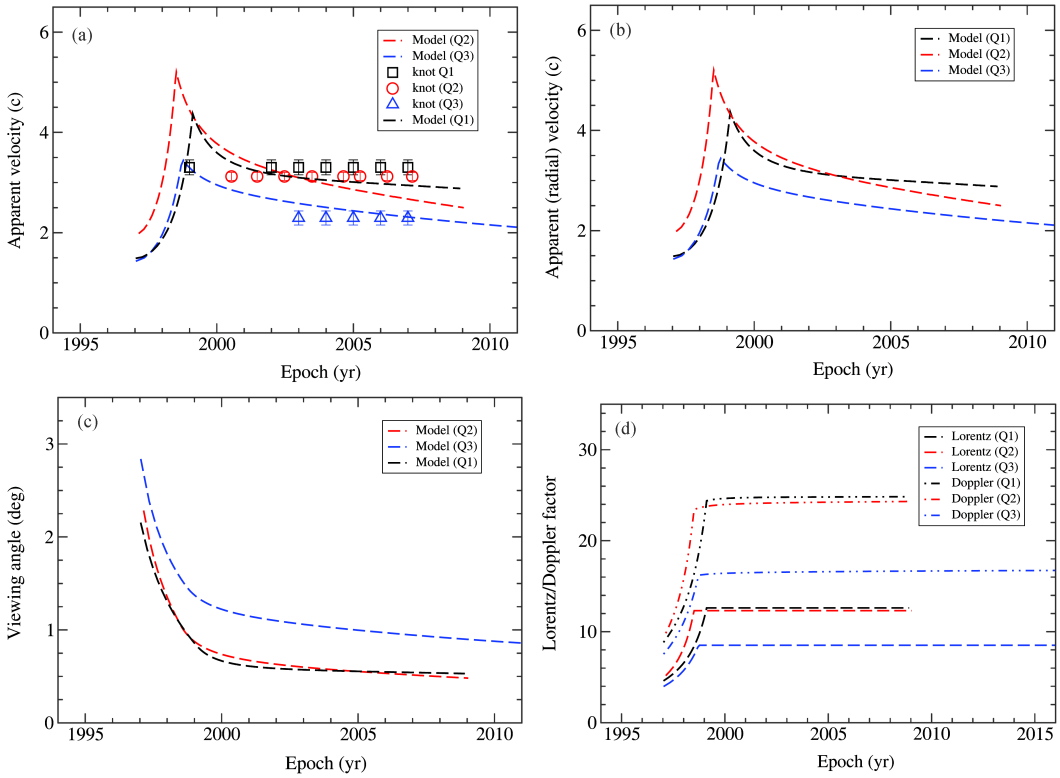

Fig. 5 Fitting results for $\epsilon = 0.12^\circ$. Apparent total and radial velocity, modeled viewing angle and Lorentz/Doppler factor are shown.

Table 1 Results on extended acceleration of the knots for cases of $\epsilon = 6^\circ$, 3°, 1°, 0.6° and 0.12°: maximum (radial) distance of acceleration region ($Z_{\max}$), initial and maximum Lorentz factor Γ_i and $\Gamma_{\max}$ respectively, and corresponding maximum Doppler factor ($\delta_{\max}$).

ϵ (deg)	knot	$Z_{\max}$ (pc)	Γ_i	$\Gamma_{\max}$	$\delta_{\max}$
6	Q1	4.0	1.4	3.0	4.1
	Q2	–	3.4	3.4	–
	Q3	4.0	1.4	2.6	3.5
3	Q1	6.8	1.5	4.0	6.1
	Q2	–	3.7	3.7	–
	Q3	4.2	1.5	2.7	3.6
1	Q1	17	3.0	5.5	9.8
	Q2	25	3.8	5.5	9.6
	Q3	17	3.1	3.6	6.2
0.6	Q1	17	3.0	6.5	12
	Q2	25	3.8	6.6	12
	Q3	17	3.1	4.6	8.3
0.12	Q1	34	3.5	12.6	24
	Q2	25	3.8	12.3	23
	Q3	17	3.1	8.5	16

been observed in blazars (e.g.) 3C345 and 3C279 and is predicted by some theories of relativistic magnetohydrodynamics (MHD) related to the formation of relativistic jets (Vlahakis & Königl 2004, Vlahakis 2006, Komissarov et al. 2007, Tchekhovskoy et al. 2010). Thus our results from the model-fitting simulations on the kinematics of the superluminal knots in NRAO 150 can be regarded as additional evidence for extended intrinsic acceleration that occurred in the inner jets of blazars.

For understanding the jet position angle swing observed in blazar 3C345, Qian et al. (1992, 2009) proposed a scenario with a precessing jet nozzle or precessing helical trajectory model, and the position angle swings observed in blazars 3C279 (Qian 2012, 2013) and 3C454.3 (Qian et al. 2014) can also be interpreted in this framework during certain periods. However, position angle swings in blazars seem not to be a single phenomenon and long-term regular swings could only be discerned in some cases.

Based on their new multi-frequency polarimetric VLBI observations, Molina et al. (2013, 2014) proposed a helical motion scenario to interpret the jet position angle swing and non-ballistic motion observed in NRAO 150, showing that internal rotation of the jet material around the jet axis (assuming the jet is viewed faced on) could be the cause of the swing and make it an alternative explanation for the position angle swing originating from instabilities in the jet. The circular structure of the toroidal field component observed in the innermost regions provides some evidence for the helical magnetic field structure there. They demonstrate that the helical trajectories of the knots could have originated at different distances from the jet axis with different helical patterns.

Based on our previous model-fitting simulations on the jet position angle swings in blazars 3C345, 3C279 and 3C454.3, in our model we assume that all the observed trajectories of the knots originated from a common helical path which precesses around the (mean) jet axis, as in the scenarios proposed for explaining the position angle swings observed in blazars 3C279 (Qian 2011, 2012, 2013), 3C454.3 (Qian et al. 2014) and 3C345 (Qian et al. 1992, Qian et al. 2009). Therefore, the precessing nozzle scenario we suggested could be applied to interpret the ejection position angle swings and the rotation of the inner trajectory in a few blazars (redshift z from $\sim$0.5 to $\sim$1.5) and extended intrinsic acceleration could also be studied.

Therefore, both model-fitting results argue that the jet position angle swing and non-ballistic motion observed in this high-redshift quasar NRAO 150 may be due to helical motion plus precession of the jet nozzle, not due to erratic jet wobbling caused by instabilities in the jet and/or disk. Magnetic fields may play an important role in the dynamics of the jet associated with NRAO 150. However, available observations in some blazars have revealed that the pattern of jet swing behavior could largely change during different periods, e.g. in 3C279 and OJ287 (the so called "PA jump," see Qian 2013, Lu et al. 2013, Tateyama & Kingham 2004 and Agudo et al. 2012). The cause is still unclear. NRAO 150 is an exceptional source and it is important to do further mm-VLBI monitoring to see whether this regular precessing helical motion with an extremely curved trajectory could continue to occur. Recently, general relativistic MHD simulations (e.g., McKinney et al. 2013, Dexter et al. 2014, Tchekhovskoy et al. 2014) show that both jet precession and erratic jet wobbling could occur in the so-called "magnetically arrested disk" case, largely depending on the state of the mass and magnetic field accretion (including inversion of field direction) onto the black hole. NRAO 150 might be an exceptional source and it is important to make further mm-VLBI monitoring to see whether this regular precessing helical motion with extremely curved trajectory could continue to occur.

Jet position angle swing may not be a single phenomenon and it could contain (at least) four components (ingredients): (1) long-term, quasi-periodic behavior, possibly caused by precession; (2) erratic swing caused by jet/disk instabilities; (3) sudden position angle jumps possibly caused by a sudden change of the jet direction; (4) jet oscillations caused by instabilities due to the interaction of the jet with its environment.

Our model assumes the superluminal knots are moving along a common helical trajectory which regularly precesses around the jet-axis (i.e. a precessing helical jet nozzle model). Both precession and helical motion have been investigated by many authors. Magnetohydrodynamical theories for the formation/acceleration/collimation of relativistic jets predict helical motion of knots and jet precession caused by the supermassive black hole/accretion disk system in the central engine (Vlahakis & Königl 2004, Vlahakis 2006, Komissarov et al. 2007, Tchekhovskoy et al. 2010, Camenzind & Krockenberger 1992, Steffen et al. 1995, Schramm et al. 1993, Koenigl & Choudhuri 1985, Caproni & Abraham 2004, Liu & Melia 2002, Lobanov & Roland 2005). Since the precessing nozzle (or precessing trajectory) model originally suggested for 3C345 by Qian et al. (1991) has also been applied to interpret the position angle swings and pc-scale kinematics of the superluminal components observed in several blazars: 3C345 (Qian et al. 1991, 2009); 3C454.3 (Qian et al. 2014); 3C279 (Qian 2011, 2012, 2013); NRAO 150 (this paper), the ejection of superluminal components by a precessing-nozzle could be a common phenomenon in blazars. In fact in literature there are more blazars that have this behavior: e.g. OJ287 (Tateyama & Kingham 2004) and BL Lacertae (Stirling et al. 2003), at least during some periods.

We would point out that this phenomenon could be understood in terms of the theories of relativistic MHD for the formation-collimation-acceleration of relativistic jets (e.g., Blandford & Znajek 1977, Blandford & Payne 1982, Li et al. 1992, Meier 1999, Vlahakis & Königl 2004, Vlahakis 2006, Komissarov et al. 2007, Tchehovskoy et al. 2010, Camenzind 1990, Camenzind & Krockenberger 1992, Steffen et al. 1995, Schramm et al. 1993, Königl & Choudhouri 1985, Caproni 2004, Liu & Melia 2002, Lobanov & Roland 2005).

Firstly, studies of relativistic MHD (e.g., Blandford & Znajek 1977, Li et al. 1992, Vlahakis & Königl 2004, Vlahakis 2006, Millas et al. 2014) have shown that a magnetic-nozzle could be formed in the disk-driven jet in the rotating black-hole/disk magnetosphere and it is located near the classical fast magnetosonic point where the flow remains Poynting flux dominated. Beyond this point the jet enters into the acceleration region until approaching the modified fast-magnetosonic point. Due to the classical fast-magnetosonic point being located in the force-free region of the magnetosphere where the plasma is highly magnetized, both the magnetic field lines of the jet (anchored in the innermost disk) and the magnetic nozzle would rotate rigidly with the disk (e.g., Macdonald & Thorne 1982). As the normal of the disk is inclined to the spin axis of the black hole with a small angle, its innermost part could be dragged to be precessing around the spin axis

of the black hole by the Lense-Thirring effect (Qian et al. 2014). This explains the existence of the precessing nozzle and the periodic ejection of superluminal components in blazars.

Secondly, because the jet is still magnetically dominated at the classical fast magnetosonic point and there is ample electromagnetic energy (Poynting flux) to be transformed to plasma kinetic energy, the jet could be greatly accelerated beyond the classical fast-magnetosonic point (or between the classical and modified fast magnetosonic points). This is the so-called "extended bulk acceleration" in blazar jets. In this acceleration region the inertia of the plasma is strong and the electromagnetic fields are neither degenerate nor force-free. The plasmas would flow on the magnetic surfaces along their own streamlines which are distinct from the field lines and they have helical patterns with pitch angles different from that of the field lines. As widely studied, in the axisymmetric black-hole/disk magnetosphere and the streamlines of the plasma flow are generally axisymmetric. Thus the components ejected from the magnetic nozzle at different times would follow self-similar trajectories, illuminating their respective streamlines and creating their own channel/trajectory (or magnetic tubes). This explains why the superluminal components observed with VLBI move along a precessing common trajectory.

Therefore we conclude that the precessing nozzle (trajectory) model, which we have used to perform model-fitting of the position angle swings and kinematics at pc-scales observed in several blazars, can be understood in terms of the theory of relativistic MHD for relativistic jets. That is, the phenomena observed at pc-scales with VLBI is consistent with the black hole physics and relativistic magnetohydrodynamics for jet formation.

Acknowledgements I wish to thank the anonymous referee for the constructive comments which were helpful for improving the presentation of the results. I would also like to thank Prof. Tsien S.C. for his encouragement and lasting support of my research on blazar phenomena.

Appendix A: MODEL FITTING RESULTS FOR $\epsilon = 6^\circ$, 1° AND 0.6°

Results for ϵ = 6°

The parameters used for the model-fitting are: $Z_1 = 18$ mas, $Z_2 = 1.0$ mas.

The amplitude and precession phase functions are described by Equations (14) and (15) shown above. The respective model parameters for knots Q1, Q2 and Q3 are given as follows.

- Knot Q1: Ejection epoch t_0 = 1993.4, ϕ = 4.0 rad, η = 1. The bulk Lorentz factor Γ is chosen as: (1) for $Z \leq 0.47$ mas, $\Gamma = 1.4 + (3.0 - 1.4)(Z/0.47)$ (initial bulk acceleration); (2) for $Z > 0.47$ mas, Γ = 3.0.
- Knot Q2: Ejection epoch t_0 = 1996.0, ϕ = 2.7 rad, η = 1. The Lorentz factor Γ = 3.4 (no initial bulk acceleration).
- Knot Q3: Ejection epoch t_0 = 1994.60 (i.e. before knot Q2), ϕ = 3.4 rad, η = 2.3 (larger rotation rate than for Q1 and Q2). The initial bulk acceleration is described as: (1) for $Z \leq 0.47$ mas, $\Gamma = 1.4 + (2.6 - 1.4)(Z/0.47)$, (2) for $Z > 0.47$ mas Γ = 2.6.

The model-fitting results are shown in Figures A.1 and A4. For knots Q1 and Q3 intrinsic bulk acceleration is required during the initial part of their trajectory. The trajectory (including (X_n, Z_n), X_n(t) and Z_n(t)), core distance and apparent velocity (including both total and radial velocity) are reasonably and consistently well fitted by the model. The bulk Lorentz factor is fitted in the range of $\sim$1.5–3.5. The period of precession is derived to be 12.57 yr. In this case the modeled viewing angle is in the range of 10°–30° which seems too large, because the required bulk Lorentz factor Γ seems too small and any independent determination of the Lorentz/Doppler factor (e.g. from mm-flare activity) would be helpful.

Results for ϵ = 1°

The parameters used for the model-fitting are: Z_1 = 60 mas and Z_2 = 3 mas. The amplitude and phase functions are described by Equations (14) and (15) as shown before. The respective model parameters for knots Q1, Q2 and Q3 are given as follows.

- Knot Q1: Ejection epoch t_0 = 1995.50, ϕ = 4.0 rad and η = 1. Intrinsic acceleration is assumed as: (1) for $Z \leq 2.0$ mas $\Gamma = 3.0 + (5.5 - 3.0)Z/2.0$; (2) for $Z > 2.0$ mas Γ = 5.5.
- Knot Q2: Ejection epoch t_0 = 1996.0, ϕ = 2.8 rad, η = 1. Intrinsic acceleration is assumed as: (1) for $Z \leq 3.0$ mas $\Gamma = 3.8 + (5.5 - 3.8)Z/3.0$; (2) for $Z > 3.0$ mas Γ = 5.5.
- Knot Q3: Ejection epoch t_0 = 1995.65, ϕ = 3.64 rad, η = 2.3 (larger rotation rate than for knot Q1 and Q2). Intrinsic acceleration is assumed as: (1) for $Z \leq 2.0$ mas $\Gamma = 3.1 + (3.6 - 3.1)Z/2.0$; (2) for $Z > 2.0$ mas Γ = 3.6.

The fitting results are shown in Figures A2 and A5. It can be seen that the trajectory, core distance and apparent velocity are reasonably and consistently well fitted. The modeled Lorentz factor is in the range of $\sim$3–5 and the Doppler factor is in the range of $\sim$5–10. The modeled viewing angle is in the range of $\sim 3^\circ$–8°. In this case the precession period is derived as 2.62 yr.

Results for ϵ = 0.6°

We chose the fitting parameters as: $Z_1 = 100$ mas and $Z_2 = 5.0$ mas. The amplitude and phase functions are described by Equations (14) and (15) as shown before. The respective model parameters for knots Q1, Q2 and Q3 are given as follows.

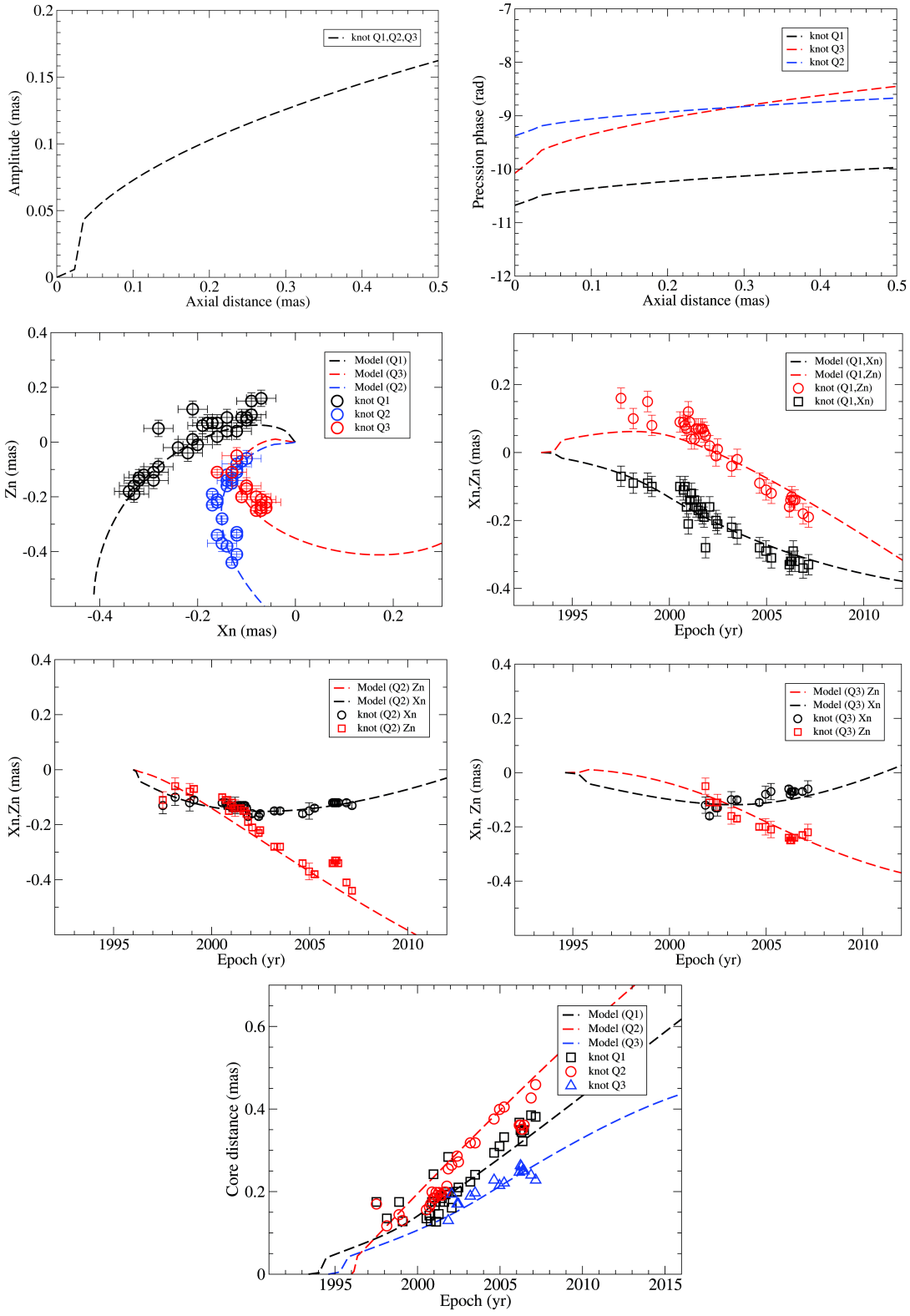

Fig. A.1 Fitting results for $\epsilon = 6°$. Amplitude $A(Z)$ and phase $\Phi(Z)$, trajectory (X_n, Z_n), $X_n(t)$ and $Z_n(t)$ (respectively for Q1, Q2 and Q3), and core distance.

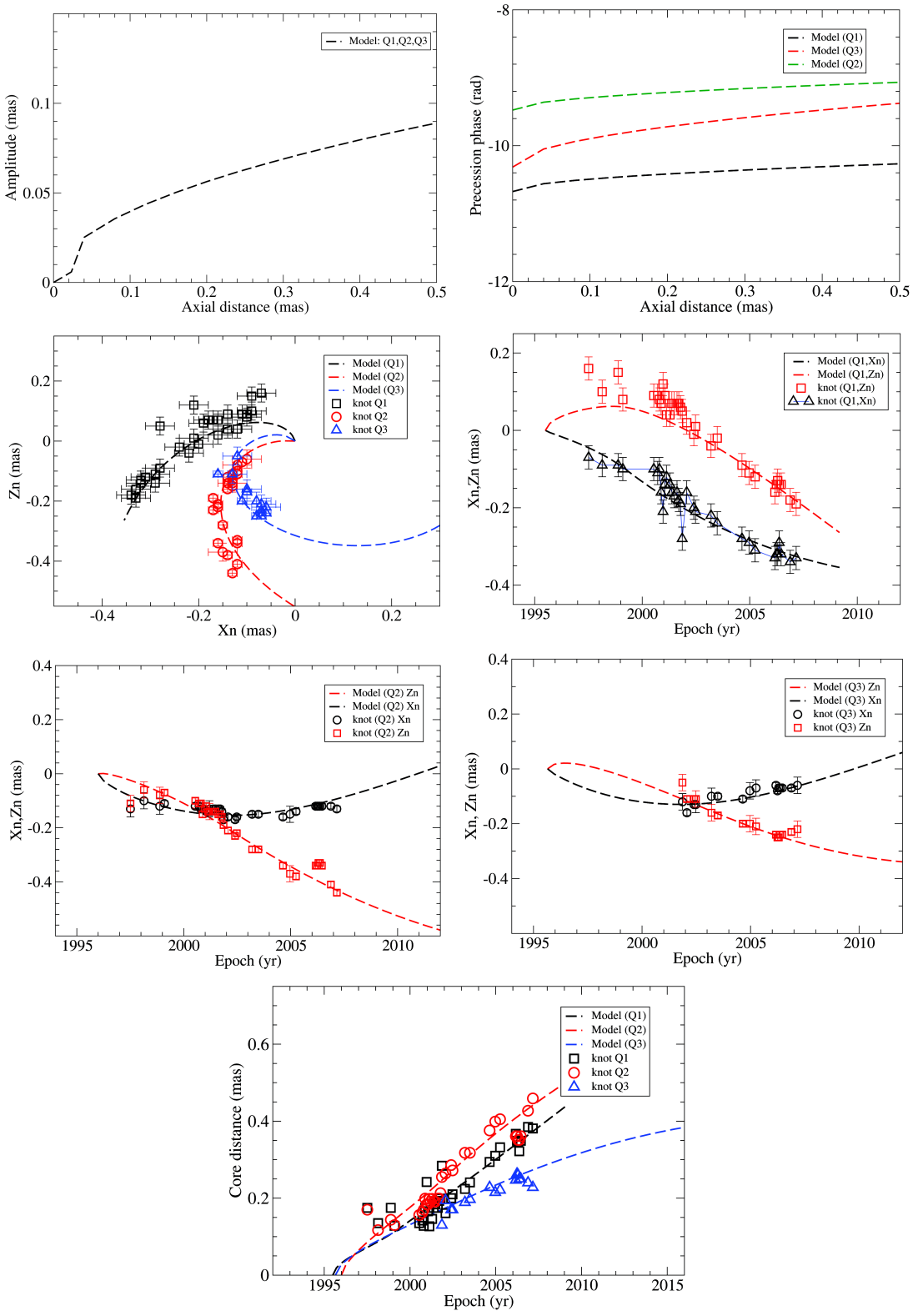

Fig. A.2 Fitting results for $\epsilon = 1°$. Amplitude $A(Z)$ and phase $\Phi(Z)$, trajectory (X_n, Z_n), $X_n(t)$ and $Z_n(t)$ (respectively for Q1, Q2 and Q3), and core distance.

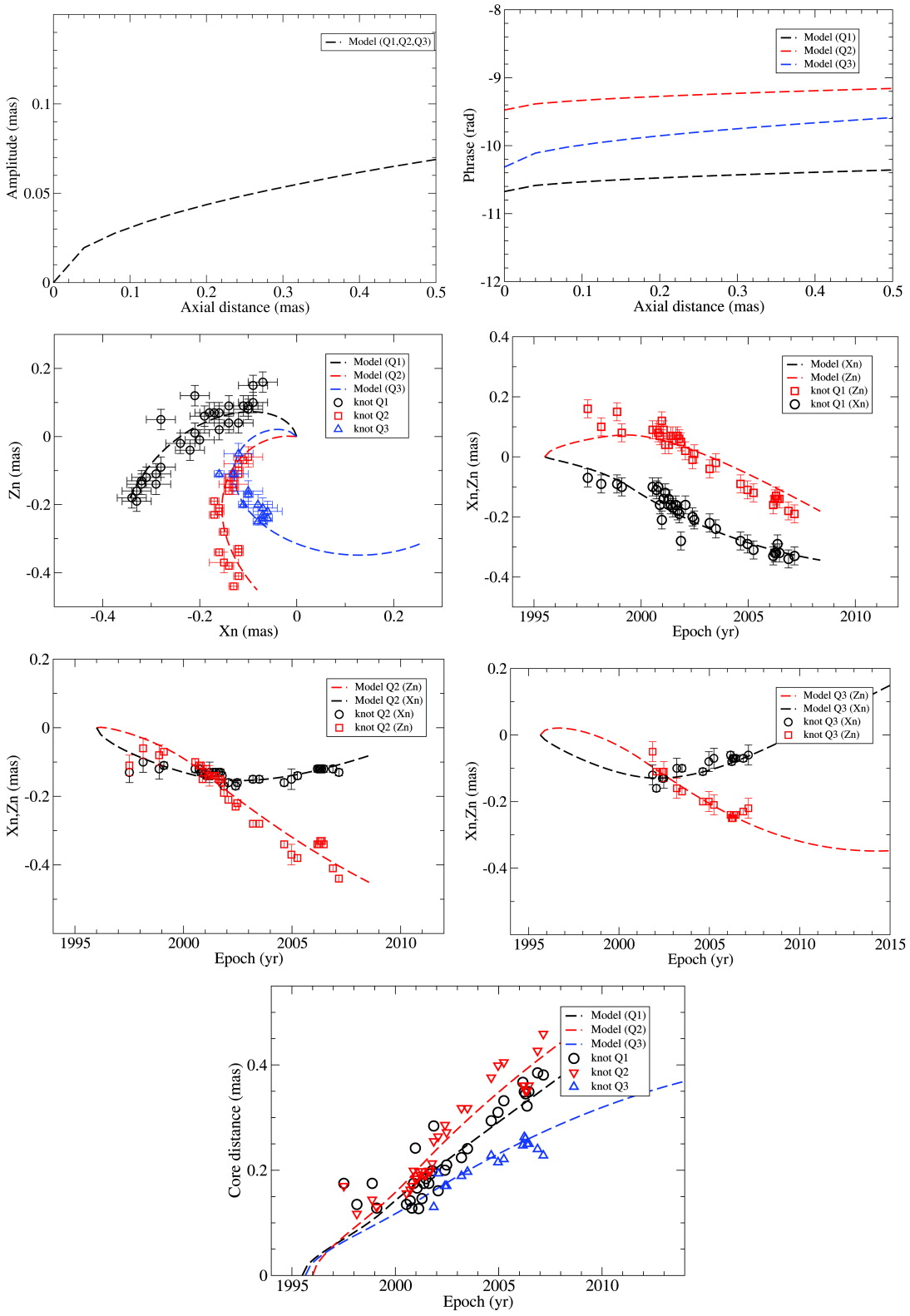

Fig. A.3 Fitting results for $\epsilon = 0.6°$. Amplitude $A(Z)$ and phase $\Phi(Z)$, trajectory (X_n, Z_n), $X_n(t)$ and $Z_n(t)$ (respectively for Q1, Q2 and Q3), and core distance.

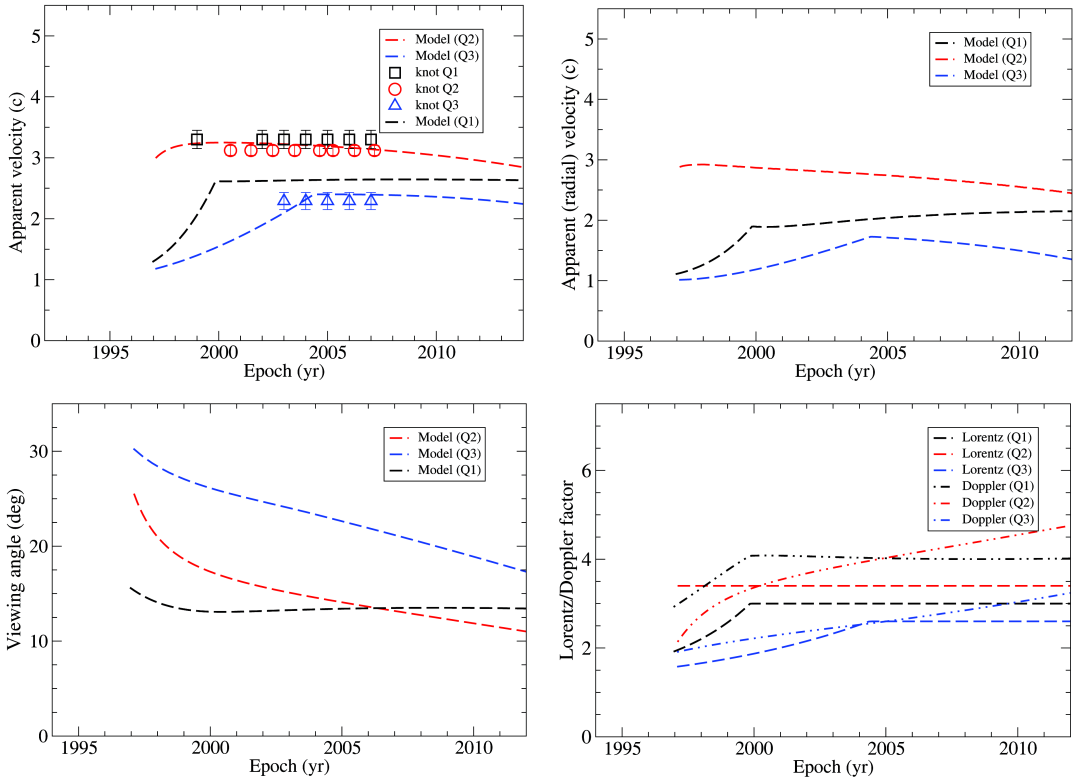

Fig. A.4 Fitting results for $\epsilon = 6^\circ$. Apparent total and radial velocity, modeled viewing angle and Lorentz/Doppler factor.

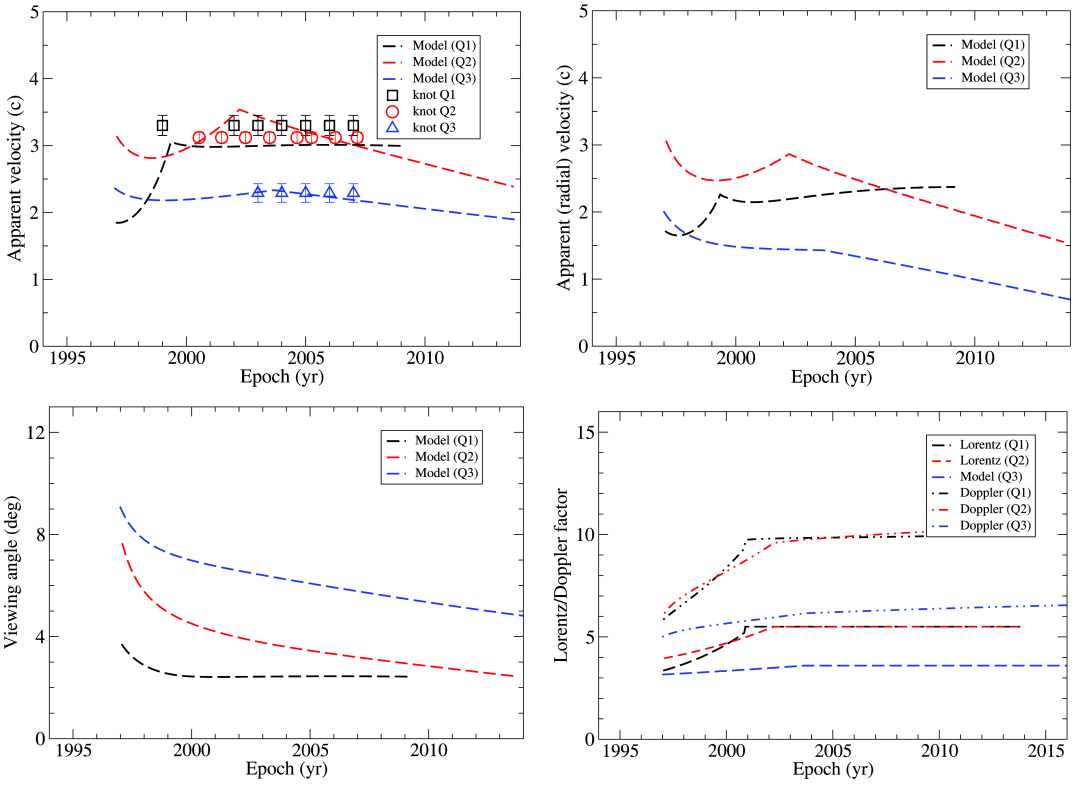

Fig. A.5 Fitting results for $\epsilon = 1^\circ$. Apparent total and radial velocity, modeled viewing angle and Lorentz/Doppler factor.

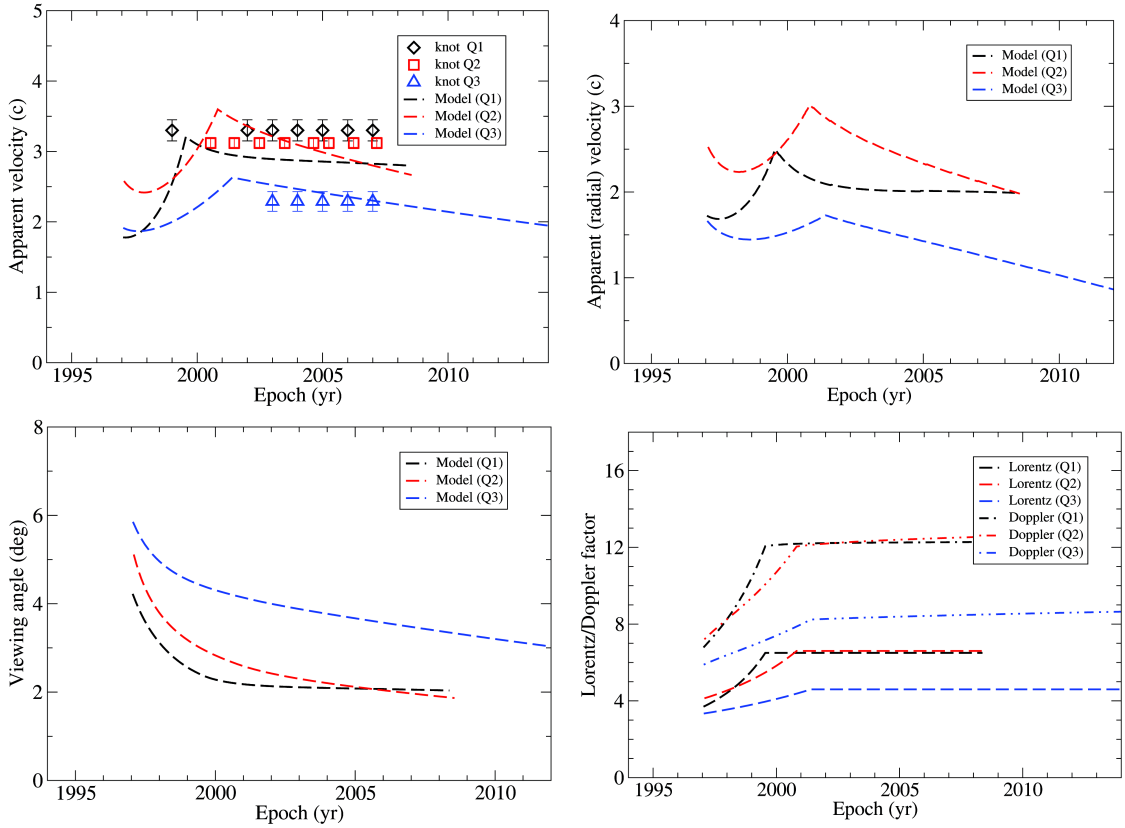

Fig. A.6 Fitting results for $\epsilon = 0.6°$. Apparent total and radial velocity, modeled viewing angle and Lorentz/Doppler factor.

– Knot Q1: Ejection epoch t_0 = 1995.50, ϕ = 4.0 rad, η = 1. Intrinsic acceleration is chosen as: (1) for $Z \leq 2.0$ mas $\Gamma = 3.0 + (6.5 - 3.0)Z/2.0$; (2) for $Z > 2.0$ mas Γ = 6.5.
– Knot Q2: Ejection epoch t_0 = 1996.0, ϕ = 2.8 rad, η = 1. The intrinsic acceleration is chosen as: (1) for $Z \leq 3.0$ mas $\Gamma = 3.8 + (6.6 - 3.8)Z/3.0$; (2) for $Z > 3.0$ mas Γ = 6.6.
– Knot Q3: Ejection epoch t_0 = 1995.65, ϕ = 3.64, η = 2.3 (more rotation than for Q1 and Q2). Intrinsic acceleration is assumed as: (1) for $Z \leq 2.0$ mas $\Gamma = 3.1 + (4.6 - 3.1)Z/2.0$; (2) for $Z > 2.0$ mas Γ = 4.6.

The model fitting results are shown in Figures A3 and A6. It can be seen that the trajectory, core distance and apparent velocity are all reasonably and consistently well fitted. The modeled Lorentz factor is in the range of ∼3.5–6.5 and Doppler factor in the range of ∼9–12. The viewing angle is derived to be in the range of $2°$–$6°$. The precession period is derived to be 2.62 yr.

References

Acosta-Pulido, J. A., Agudo, I., Barrena, R., et al. 2010, A&A, 519, A5
Agudo, I. 2009, in Astronomical Society of the Pacific Conference Series, 402, Approaching Micro-Arcsecond Resolution with VSOP-2: Astrophysics and Technologies, ed. Y. Hagiwara, E. Fomalont, M. Tsuboi, & M. Yasuhiro, 330
Agudo, I., Marscher, A. P., Jorstad, S. G., et al. 2012, ApJ, 747, 63
Agudo, I., Bach, U., Krichbaum, T. P., et al. 2007, A&A, 476, L17
Blandford R. D. & Znajek R. L., 1977, MNRAS, 179, 433
Blandford R. D., & Payne D. G. 1982, MNRAS, 199, 883
Camenzind M., 1990, Reviews in Modern Astronomy (Berlin: Springer-Verlag), 3, 234
Camenzind, M., & Krockenberger, M. 1992, A&A, 255, 59
Caproni, A., & Abraham, Z. 2004, ApJ, 602, 625
Dexter J., McKinney J. C., Markoff S., Tchekhovskoy A., 2014, MNRAS 440, 2185 (arXiv-1312.1691)
Fey, A. L., & Charlot, P. 2000, ApJS, 128, 17
Hogg, D. W. 1999, astro-ph/9905116
Koenigl, A., & Choudhuri, A. R. 1985, ApJ, 289, 173
Komissarov, S. S., Barkov, M. V., Vlahakis, N., & Königl, A. 2007, MNRAS, 380, 51
Li Z. Y., Chieuh Z. H., Begelman M. C., 1992, ApJ 394, 459
Lister, M. L., Kellermann, K. I., Vermeulen, R. C., et al. 2003, ApJ, 584, 135
Liu, S., & Melia, F. 2002, ApJ, 573, L23
Lobanov, A. P., & Roland, J. 2005, A&A, 431, 831
Lu, R.-S., Fish, V. L., Akiyama, K., et al. 2013, ApJ, 772, 13
Macdonald D., Thorne K. S., 1982, MNRAS 198, 345

McKinney J. C., Tchekhovskoy A., Blandford R.D., 2014, Science 339, 49 (arXiv-1211.3651)
Meier D.L., 1999, ApJ 522, 753
Millas D., Katsoulakos G., Lingri D., et al., High Energy Phenomena In Relativistic Outflows, Interntional Journal of Modern Physics: Conference series, vol.28,1460200
Molina, S. N., Agudo, I., & Gómez, J. L. 2013, in European Physical Journal Web of Conferences, 61, European Physical Journal Web of Conferences, 8003
Molina, S. N., Agudo, I., Gómez, J. L., et al. 2014, A&A, 566, A26
Pen, U.-L. 1999, ApJS, 120, 49
Qian, S.-J. 2011, RAA (Research in Astronomy and Astrophysics), 11, 43
Qian, S.-J. 2012, RAA (Research in Astronomy and Astrophysics), 12, 46
Qian, S.-J. 2013, RAA (Research in Astronomy and Astrophysics), 13, 783
Qian, S.-J., Britzen, S., Witzel, A., et al. 2014, RAA (Research in Astronomy and Astrophysics), 14, 249
Qian, S. J., Witzel, A., Krichbaum, T., et al. 1992, Chinese Astronomy and Astrophysics, 16, 137 (Translation of Acta Astronomica Sinica, vol. 32, no. 4, 1991, 369)
Qian, S.-J., Witzel, A., Zensus, J. A., et al. 2009, RAA (Research in Astronomy and Astrophysics), 9, 137
Schramm, K.-J., Borgeest, U., Camenzind, M., et al. 1993, A&A, 278, 391
Spergel, D. N., Verde, L., Peiris, H. V., et al. 2003, ApJS, 148, 175
Steffen, W., Zensus, J. A., Krichbaum, T. P., Witzel, A., & Qian, S. J. 1995, A&A, 302, 335
Stirling, A. M., Cawthorne, T. V., Stevens, J. A., et al. 2003, MNRAS, 341, 405
Tateyama, C. E., & Kingham, K. A. 2004, ApJ, 608, 149
Tchekhovskoy A., Metzger B. D., Giannios D., Kelley L. Z., 2014, MNRAS 437, 2744 (arXiv-1301.1982)
Tchekhovskoy, A., Narayan, R., & McKinney, J. C. 2010, ApJ, 711, 50
Villata, M., & Raiteri, C. M. 1999, in Astronomical Society of the Pacific Conference Series, 159, BL Lac Phenomenon, ed. L. O. Takalo & A. Sillanpää, 489
Villata, M., Raiteri, C. M., Sillanpaa, A., & Takalo, L. O. 1998, MNRAS, 293, L13
Vlahakis, N. 2006, in Astronomical Society of the Pacific Conference Series, 350, Blazar Variability Workshop II: Entering the GLAST Era, ed. H. R. Miller, K. Marshall, J. R. Webb, & M. F. Aller, 169
Vlahakis, N., & Königl, A. 2004, ApJ, 605, 656